An acoustic-transport splitting method for the barotropic Baer-Nunziato two-phase flow model

Katia Ait-Ameur, Samuel Kokh, Marica Pelanti, Marc Massot, Teddy Pichard

ESAIM: PROCEEDINGS AND SURVEYS, Vol. ?, 2022, 1-10
Editors: Will be set by the publisher

AN ACOUSTIC-TRANSPORT SPLITTING METHOD FOR THE BAROTROPIC BAER-NUNZIATO TWO-PHASE FLOW MODEL *

Katia Ait-Ameur[1], Samuel Kokh[2], Marica Pelanti[3], Marc Massot[1] and Teddy Pichard[1]

Abstract. This work focuses on the numerical approximation of the barotropic Baer-Nunziato two-phase flow model. The scheme relies on an operator splitting method corresponding to a separate treatment of fast propagation phenomena due to the acoustic waves on the one hand and slow propagation phenomena due to the fluid motion on the other. We propose to extend the implicit-explicit schemes developed in [7]. These methods enable the use of time steps that are no longer constrained by the sound velocity thanks to an implicit treatment of the acoustic waves, and maintain accuracy in the subsonic regime thanks to an explicit treatment of the material waves. In the present setting, a particular attention will be also given to the discretization of the non conservative terms in the Baer-Nunziato model. We prove that the proposed numerical strategy preserve positive values of the volume fractions and densities and we illustrate its behaviour with several relevant test cases.

Résumé. Ce travail porte sur l'approximation numérique du modèle de Baer-Nunziato barotrope. Le schéma se base sur une méthode de splitting correspondant à un traitement séparé des ondes acoustiques d'une part et des ondes matières d'autre part. Nous proposons d'étendre les schémas implicites-explicites développés dans [7]. Ces méthodes permettent d'utiliser des pas de temps qui ne sont plus contraints par la vitesse du son grâce à un traitement implicite des ondes acoustiques, et de conserver une précision dans le régime subsonique grâce à un traitement explicite des ondes matières. Dans ce travail, une attention particulière sera également portée à la discrétisation des termes non conservatifs dans le modèle de Baer-Nunziato. Nous montrons que les méthodes numériques proposées préservent la positivité des densités et des fractions volumiques et nous illustrons leurs comportements à l'aide de plusieurs cas tests représentatifs des difficultés numériques liées à ce modèle.

1. Introduction

We are interested in the computation of compressible two-phase flows with the two-fluid Baer-Nunziato (BN) model [4]. From a numerical point of view, the BN model raises some issues. One difficulty comes from the presence of non conservative products and more precisely the fact that the model cannot be equivalently recast in full conservative form. However, the non conservative products naturally vanish when the void fractions α_k are locally constant in space, and the model coincides in that case with two (decoupled) gas dynamics systems.

* *This work was supported by a grant from Region Ile-de-France DIM MATHINNOV and the DGA project MMEED.*

[1] CMAP, CNRS, École polytechnique, Institut Polytechnique de Paris, 91120 Palaiseau, France; e-mail: katia.ait-ameur@polytechnique.edu, marc.massot@polytechnique.edu, teddy.pichard@polytechnique.edu

[2] CEA-DES/ISAS/DM2S/STMF/LMEC, CEA Saclay, Gif-sur-Yvette, 91191, France; e-mail: samuel.kokh@cea.fr

[3] IMSIA, ENSTA Paris - EDF - CNRS - CEA, Institut Polytechnique de Paris, 828, Boulevard des Maréchaux, Palaiseau, 91120, France; e-mail: marica.pelanti@ensta-paris.fr

A second difficulty is related to the total boiling or condensation of one phase that arise a singularity in the model. The absent phase is called vanishing phase or ghost phase. It poses a difficulty in the two-fluid model for the computation of the velocity for the ghost phase. Several schemes have already been proposed in the literature in order to build consistent and stable approximations of the Baer-Nunziato model, among which we may cite those relying on time-explicit, exact or approximate Riemann solver (see for instance [2,3,17,21]). We also mention some other finite volume techniques that have been used. In [14], the authors extend Rusanov's scheme and the VFRoe method to the context of non conservative systems. Other schemes rely on relaxation techniques (see for instance [1,12]).

For stability reasons, the time steps Δt involved in such methods are subject to a usual CFL condition that depends on the material velocities and the sound speeds. It is then clear that the definition of Δt is driven by the fastest eigenvalues, associated with the acoustic waves. In many applications, the acoustic waves are not predominant physical phenomena. A CFL condition based on the most influent waves, the contact waves associated to the material velocities would be more adapted. The idea is then to propose a time-implicit treatment of the acoustic waves, in order to get rid of a too restrictive CFL condition, together with an explicit treatment of the contact waves in order to preserve accuracy. This idea has already been used earlier within the framework of Euler equations and Shallow Water equations (see for instance [7,9,13]) using a Lagrange-Projection approach, but also for two-phase flows models (see [5,8,11,16,19,22]).

The paper is organized as follows. In Section 2, we present the set of partial differential equations of the Baer-Nunziato two-phase flow model in the barotropic framework, and we recall its main mathematical properties. In Section 3, we propose an operator splitting method for this model, and, in Section 4, we describe the numerical treatment of each step. In Section 5, we build an explicit and semi-implicit numerical schemes based on this operator splitting method for the solution of the Baer Nunziato model. Finally, Section 6 is devoted to the numerical experiments, where representative test cases have been implemented.

2. The Baer-Nunziato model

In the present work, we consider the compressible barotropic one-dimensional BN model where balance equations account for the evolution of mass and momentum of each phase. There are five unknowns that describe the evolution of the two-phase flow: the velocities of each phase u_k, where $k \in \{1,2\}$, the densities of each phase ρ_k and the phase fractions α_k (knowing that $\alpha_1 + \alpha_2 = 1$). We also assume a barotropic pressure law for each phase $\rho_k \to p_k(\rho_k), k \in \{1,2\}$ such that the sound speed is defined by $c_k^2 = p_k'(\rho_k) > 0$. The 1D barotropic BN model reads:

$$\left\{\begin{array}{lcll} \partial_t \alpha_1 & + & u_I \partial_x \alpha_1 & = 0, \\ \partial_t(\alpha_1\rho_1) & + & \partial_x(\alpha_1\rho_1 u_1) & = 0, \\ \partial_t(\alpha_1\rho_1 u_1) & + & \partial_x(\alpha_1\rho_1 u_1^2 + \alpha_1 p_1) - p_I \partial_x \alpha_1 & = 0, \\ \partial_t(\alpha_2\rho_2) & + & \partial_x(\alpha_2\rho_2 u_2) & = 0, \\ \partial_t(\alpha_2\rho_2 u_2) & + & \partial_x(\alpha_2\rho_2 u_2^2 + \alpha_2 p_2) - p_I \partial_x \alpha_2 & = 0, \end{array}\right. \tag{1}$$

where u_I and p_I are the interfacial velocity and pressure for which one must provide closure laws. So far as the definitions of u_I and p_I are concerned, we first observe that the characteristic speeds of (1) are always real and given by $Sp = \{u_I, u_k \pm c_k, \quad k = 1,2\}$, where c_k denotes the speed of sound in phase k. When (1) is hyperbolic, one can easily check that similarly to the classical gas dynamics equations, the characteristic fields associated with the eigenvalues $u_k \pm c_k$ are genuinely nonlinear. Regarding the characteristic field associated with u_I, it is generally required to be linearly degenerate in practice. This property holds as soon as

$$u_I = \beta u_1 + (1-\beta)u_2, \quad \beta = \frac{\chi\alpha_1\rho_1}{\chi\alpha_1\rho_1 + (1-\chi)\alpha_2\rho_2}, \tag{2}$$

where $\xi \in [0,1]$ is a constant (we refer to [14] for the details). Regarding the interfacial pressure p_I , we set $p_I = \mu p_1 + (1-\mu)p_2, \mu \in [0,1]$. In the last section, dedicated to the numerical results, the pair of interfacial velocity and pressure will be given by: $\chi = 0, \mu = 1$ such that:

$$(u_I, p_I) = (u_2, p_1). \tag{3}$$

We denote $\mathbb{U} = (\alpha_1, \alpha_1\rho_1, \alpha_1\rho_1 u_1, \alpha_2\rho_2, \alpha_2\rho_2 u_2)$ the unknown vector which is expected to belong to the set of admissible states:

$$\Omega = \left\{ \mathbb{U} \in \mathbb{R}^5, \quad 0 < \alpha_k < 1, \quad \rho_k > 0, \quad k \in \{1,2\}, \quad \alpha_1 + \alpha_2 = 1 \right\}. \tag{4}$$

System (1) takes the following condensed form

$$\partial_t \mathbb{U} + \partial_x F(\mathbb{U}) + C(\mathbb{U})\partial_x \mathbb{U} = 0, \quad x \in \mathbb{R}, \quad t > 0, \tag{5}$$

where

$$F(\mathbb{U}) = \begin{pmatrix} 0 \\ \alpha_1\rho_1 u_1 \\ \alpha_1\rho_1 u_1^2 + \alpha_1 p_1(\rho_1) \\ \alpha_2\rho_2 u_2 \\ \alpha_2\rho_2 u_2^2 + \alpha_2 p_2(\rho_2) \end{pmatrix}, \quad C(\mathbb{U})\partial_x \mathbb{U} = \begin{pmatrix} u_I \partial_x \alpha_1 \\ 0 \\ -p_I \partial_x \alpha_1 \\ 0 \\ -p_I \partial_x \alpha_2 \end{pmatrix}. \tag{6}$$

3. Operator splitting acoustic-transport

Before going further on, we recall that this idea has already been used earlier within the framework of Euler equations (see for instance [13]) using a Lagrange-Projection approach, but also for the Baer-Nunziato model (see [5,11]). In [5], the authors propose an operator splitting with three steps for the Baer Nunziato model with energy equations. The two first steps correspond to the acoustic and transport part of the Euler equations for each phase and the third step gathers the non conservative terms that couple the two phases. In [11], the authors propose an operator splitting in two steps where the coupling terms are distributed in the two subsytems. In this case, the transport part arises a weakly hyperbolic system and a careful treatment has to be made for the numerical discretization. In this section, we introduce an operator splitting for the barotropic BN model in two steps where the two subsystems account for the coupling terms like [11] while preserving the hyperbolicity of each subsystem like [5].
The first step corresponds to the propagation of acoustic waves:

$$\left\{ \begin{array}{lcllcll} \partial_t \alpha_1 & & & & = & 0, & \\ \partial_t m_k & + & m_k \partial_x u_k & & = & 0, & k \in \{1,2\}, \\ \partial_t (m_k u_k) & + & m_k u_k \partial_x u_k + \partial_x(\alpha_k p_k) - p_I \partial_x \alpha_k & = & 0, & k \in \{1,2\}. \end{array} \right. \tag{7}$$

The second step considers the propagation of material waves due to the fluid motion:

$$\left\{ \begin{array}{lcllcll} \partial_t \alpha_1 & + & u_I \partial_x \alpha_1 & = & 0, & & \\ \partial_t m_k & + & u_k \partial_x m_k & = & 0, & k \in \{1,2\}, \\ \partial_t (m_k u_k) & + & u_k \partial_x (m_k u_k) & = & 0, & k \in \{1,2\}. \end{array} \right. \tag{8}$$

where $m_k = \alpha_k \rho_k$.

3.1. **Properties of the acoustic sub-system**

If we note $\tau_k = \rho_k^{-1}$ the specific volume, the acoustic system (7) takes the form

$$\left\{\begin{array}{lcll} \partial_t \alpha_1 & & & = 0, \\ \rho_k \partial_t \tau_k & - & \partial_x u_k & = 0, \\ \alpha_k \rho_k \partial_t u_k & + & \partial_x(\alpha_k p_k) - p_I \partial_x \alpha_k & = 0. \end{array}\right. \tag{9}$$

The acoustic system (9) is strictly hyperbolic and the eigenstructure of the system is composed of five fields associated with the eigenvalues $\{-c_k, 0, c_k\}$. The waves associated with $\pm c_k$ are genuinely nonlinear. The wave associated with 0 is linearly degenerate.

We carry on with the approximation process of the acoustic system (7) by using a Suliciu-type relaxation approximation of (9), see [6, 10, 18]. The principle of the pressure relaxation methods consists in introducing a larger system with linearly degenerate characteristic fields so that the underlying Riemann problem is easier to solve. To do so, we introduce two new independent variable pressures π_k. While the pressures p_k verify

$$\rho_k \partial_t(\alpha_k p_k) + \alpha_k (c_k/\tau_k)^2 \partial_x u_k = 0,$$

the variables π_k are evolved according to their own partial differential equations. Within the time interval $t \in [t^n, t^n + \Delta t[$, we propose to consider the following relaxation system

$$\left\{\begin{array}{lcll} \partial_t \alpha_1 & & & = 0, \\ \rho_k \partial_t \tau_k & - & \partial_x u_k & = 0, \\ \alpha_k \rho_k \partial_t u_k & + & \partial_x(\alpha_k \pi_k) - \pi_I \partial_x \alpha_k & = 0, \\ \rho_k \partial_t(\alpha_k \pi_k) & + & \alpha_k a_k^2 \partial_x u_k & = \lambda_k \left(p_k - \pi_k\right) \rho_k \alpha_k, \end{array}\right. \tag{10}$$

where λ_k are the relaxation parameters and a_k is a constant chosen in agreement with the Whitham subcharacteristic condition

$$a_k^2 > \max_{\tau_k} \left(-\frac{\partial p_k}{\partial \tau_k}(\tau_k) \right), \quad k = 1, 2, \tag{11}$$

where the max is taken over all the specific volumes τ_k in the solution of (10). We adopt the classic method that allows to reach the regime $\lambda_k \to \infty$: at each time step, we enforce the equilibrium relation $(\pi_k)_j^n = p_k^{EOS}((\tau_k)_j^n)$ and solve (10) with $\lambda_k = 0$.
For $\lambda_k = 0$, the relaxation system can take the compact form:

$$\partial_t \mathbb{W} + \partial_x G(\mathbb{W}) = (\pi_I \partial_x \alpha_1)\, E, \tag{12}$$

where $\mathbb{W} = (\alpha_1, \tau_1, u_1, \pi_1, \tau_2, u_2, \pi_2)$, $G(\mathbb{W}) = \left(u_1, \alpha_1 \pi_1, a_1^2 u_1, u_2, \alpha_2 \pi_2, a_2^2 u_2\right)$, $E = (0, 0, 1, 0, 0, -1, 0)$. Let us discuss a few properties of (12). Straightforward computation provide the following property on the characteristic fields of the relaxation system.

Proposition 3.1. *For all state vector $\mathbb{W} = (\alpha_1, \tau_1, u_1, \pi_1, \tau_2, u_2, \pi_2)$ such that $\rho_1 > 0$ and $\rho_2 > 0$, system (12) has the following characteristic speeds:*

$$Sp = \{-a_k \tau_k, 0, a_k \tau_k, \quad k \in \{1, 2\}\}.$$

Moreover, all the characteristic fields are linearly degenerate and system (12) is hyperbolic.

3.2. **Properties of the transport sub-system**

We now consider the time evolution corresponding to the transport step. Starting from the output of the first step $\mathbb{U}^\sharp$, we want to compute the updated data at time t^{n+1}, $\mathbb{U}^{n+1}$.

$$\left\{\begin{array}{lcllcl} \partial_t \alpha_1 & + & u_I \partial_x \alpha_1 & = & 0, & \\ \partial_t m_k & + & u_k \partial_x m_k & = & 0, & k \in \{1,2\}, \\ \partial_t (m_k u_k) & + & u_k \partial_x (m_k u_k) & = & 0, & k \in \{1,2\}. \end{array}\right. \tag{13}$$

Again, straightforward computation provides:

Proposition 3.2. *For all state vector $\mathbb{W} = (\alpha_1, m_1, m_1u_1, m_2, m_2u_2)$ such that $\rho_1 > 0$ and $\rho_2 > 0$, system (13) has the following characteristic speeds:*

$$Sp = \{u_I, u_k, \quad k \in \{1,2\}\}.$$

Moreover, all the characteristic fields are linearly degenerate and system (13) is hyperbolic.

4. Discretization of the acoustic and transport sub-systems

In this section, we use the operator splitting method in order to derive an implicit-explicit numerical scheme, the aim being to approximate the solutions of the barotropic Baer Nunziato model (5). Let Δt be the time step and Δx the space step, which we assume here to be constant for simplicity in the notations. The space is partitioned into cells $C_j = [x_{j-\frac{1}{2}}, x_{j+\frac{1}{2}}]$, $\quad j \in \mathbb{Z}$ where $x_{j+\frac{1}{2}} = (j+\frac{1}{2})\Delta x$ are the cell interfaces. At the discrete times $t^n = n\Delta t$, the cell average of the solution of (5) is approximated on each cell C_j by a constant value denoted by

$$\mathbb{U}_j^n = \left((\alpha_1)_j^n, (\alpha_1\rho_1)_j^n, (\alpha_1\rho_1 u_1)_j^n, (\alpha_2\rho_2)_j^n, (\alpha_2\rho_2 u_2)_j^n\right).$$

In the following two sections, we describe the discretization strategy associated with the operator splitting method in order to calculate the values of the approximate solution at time t^{n+1}, $\left(U_j^{n+1}\right)_{j\in\mathbb{Z}}$ from those at time t^n. Section 4.1 displays the numerical treatment of the Lagrangian step (7) while section 4.2 deals with the material transport step (13).

4.1. **Treatment of the first step**

We need to propose a discretization strategy for (12). The solution of a Riemann problem for (12) consists in six constant states separated by five contact discontinuities. Unfortunately, the classic relaxation solver strategy cannot be carried on here since the solution of the Riemann problem associated with (12) cannot be defined easily. However we will see in the sequel that it is possible to derive an approximate Riemann solver for (12) using a discretization of the non conservative product that is consistent with the term $\pi_I \partial_x \alpha_k$.

Let $\Delta x_L > 0, \Delta x_R > 0$. We consider a piecewise initial data defined by:

$$\mathbb{W}_k(x, t=0) = \left\{\begin{array}{ll} (\mathbb{W}_k)_L = ((\alpha_k)_L, (\tau_k)_L, (u_k)_L, (\pi_k)_L), & \text{if } x \le 0, \\ (\mathbb{W}_k)_R = ((\alpha_l)_R, (\tau_k)_R, (u_k)_R, (\pi_k)_R), & \text{if } x > 0, \end{array}\right. \tag{14}$$

where the left and right states are defined by:

$$(\pi_k)_L = p_k^{EOS}((\tau_k)_L), \quad (\pi_k)_R = p_k^{EOS}((\tau_k)_R).$$

Note that $(\pi_k)_L$ and $(\pi_k)_R$ are at equilibrium. Let us now build an approximate Riemann solver for the relaxed acoustic system (12). We look for a function $(\mathbb{W}_k)_{RP}$ composed of six states separated by discontinuities as

follows:

$$(\mathbb{W}_k)_{RP}\left(\frac{x}{t};(\mathbb{W}_k)_L,(\mathbb{W}_k)_R\right)=\begin{cases}(\mathbb{W}_k)_L & \text{if} \quad \frac{x}{t}<-\frac{a_k}{(\rho_k)_L},\\ (\mathbb{W}_k)^\star_L & \text{if} \quad -\frac{a_k}{(\rho_k)_L}<\frac{x}{t}<0,\\ (\mathbb{W}_k)^\star_R & \text{if} \quad 0<\frac{x}{t}<\frac{a_k}{(\rho_k)_R},\\ (\mathbb{W}_k)_R & \text{if} \quad \frac{x}{t}>\frac{a_k}{(\rho_k)_R},\end{cases} \tag{15}$$

where the intermediate states are such that the following properties hold:

(1) $(\mathbb{W}_k)_{RP}$ is consistent in the integral sense with the barotropic Baer Nunziato model. More specifically in our context, if Δt is such that $\frac{a_k}{(\rho_k)_R}\Delta t\leq \min(\Delta x_L,\Delta x_R)/2$, then

$$\begin{array}{rcl} G((\mathbb{W}_k)_R)-G((\mathbb{W}_k)_L)= & - & \frac{a_k}{(\rho_k)_L}\left((\mathbb{W}_k)^\star_L-(\mathbb{W}_k)_L\right)+\frac{a_k}{(\rho_k)_R}\left((\mathbb{W}_k)_R-(\mathbb{W}_k)^\star_R\right)\\ & - & \frac{\Delta x_L+\Delta x_R}{2}\left\{\pi_I\partial_x\alpha_k\right\},\end{array} \tag{16}$$

where $\{\pi_I\partial_x\alpha_k\}$ is consistent with the non conservative term, in the sense:

$$\lim_{\substack{\Delta x_L,\,\Delta x_R\to 0,\\ (\mathbb{W}_k)_L,\,(\mathbb{W}_k)_R\to(\overline{\alpha_k},\overline{\tau_k},\overline{u_k},\overline{\pi_k})}}\{\pi_I\partial_x\alpha_k\}=\overline{\pi_I}(\partial_x\alpha_k)(\overline{\alpha_k}). \tag{17}$$

(2) We impose that $(\mathbb{W}_k)_L$ and $(\mathbb{W}_k)^\star_L$ (resp. $(\mathbb{W}_k)_R$ and $(\mathbb{W}_k)^\star_R$) verify the Rankine Hugoniot jump conditions accross $\left(-\frac{a_k}{(\rho_k)_L}\right)$-wave (resp. $\left(\frac{a_k}{(\rho_k)_R}\right)$-wave):

$$\begin{array}{rcl} \frac{a_k}{(\rho_k)_L}\left((\mathbb{W}_k)^\star_L-(\mathbb{W}_k)_L\right) & + & G((\mathbb{W}_k)^\star_L)-G((\mathbb{W}_k)_L) = 0,\\ -\frac{a_k}{(\rho_k)_R}\left((\mathbb{W}_k)_R-(\mathbb{W}_k)^\star_R\right) & + & G((\mathbb{W}_k)_R)-G((\mathbb{W}_k)^\star_R) = 0.\end{array} \tag{18}$$

(3) Similarly, across the discontinuity of velocity 0 we impose that:

$$(u_k)^\star_L=(u_k)^\star_R=(u_k)^\star,\quad (\alpha_1\pi_1)^\star_L+(\alpha_2\pi_2)^\star_L=(\alpha_1\pi_1)^\star_R+(\alpha_2\pi_2)^\star_R. \tag{19}$$

Relations (18) and (19) do not provide enough information to determine the intermediate states $(\mathbb{W}_k)^\star_L$ and $(\mathbb{W}_k)^\star_R$. Indeed, they provide only seven independent relations while we need eight quantities, namely $(u_k)^\star_L$, $(u_k)^\star_R$, $(\alpha_k\pi_k)^\star_L$ and $(\alpha_k\pi_k)^\star_R$.

We choose to add another jump relation accross the stationary discontinuity of $(\mathbb{W}_k)_{RP}$, we impose

$$(\alpha_k\pi_k)^\star_R-(\alpha_k\pi_k)^\star_L=\mathcal{M}_k, \tag{20}$$

where $\mathcal{M}_k$ is a function to be specified. Relations (16), (18), (19) and (20) lead to:

$$\begin{cases} \overline{\alpha_k}u^\star_k & = & \overline{\alpha_k u_k}-\dfrac{1}{2a_k}\Delta(\alpha_k\pi_k)+\dfrac{\mathcal{M}_k}{2a_k},\\ \pi^\star_k & = & \overline{\pi_k}-\frac{a_k}{2}\Delta u_k,\\ \overline{\alpha_k}(\pi_k)^\star_L & = & (\alpha_k)_R\pi^\star_k-\frac{\mathcal{M}_k}{2},\\ \overline{\alpha_k}(\pi_k)^\star_R & = & (\alpha_k)_L\pi^\star_k+\frac{\mathcal{M}_k}{2}.\end{cases} \tag{21}$$

We now only need to determine $\mathcal{M}_k$ such that Conditions 1), 2) and 3) are satisfied. The integral consistency requirement of Condition 1) imposes

$$\mathcal{M}_k=\{\pi_I\partial_x\alpha_k\}\,\frac{\Delta x_L+\Delta x_R}{2}. \tag{22}$$

A simple mean to comply with the conditions is to choose:

$$\mathcal{M}_k = \pi_I^{\Delta}((\mathbb{W}_k)_L,(\mathbb{W}_k)_R)\left[(\alpha_k)_R-(\alpha_k)_L\right], \tag{23}$$

where $\pi_I^{\Delta}((\mathbb{W}_k)_L,(\mathbb{W}_k)_R)$ has to be chosen such that:

$$\pi_I^{\Delta}((\mathbb{W}_k)_L,(\mathbb{W}_k)_R) \to \overline{\pi_I} \text{ if } (\pi_I)_L,(\pi_I)_R \to \overline{\pi_I}.$$

At last, we choose:

$$\pi_I^{\Delta}((\mathbb{W}_k)_L,(\mathbb{W}_k)_R) = \pi_1^{\star} = \frac{\pi_1^L+\pi_1^R}{2} - a_1\frac{\pi_1^R-\pi_1^L}{2}. \tag{24}$$

This yields that

$$\{\pi_I\partial_x\alpha_k\}((\mathbb{W}_k)_L,(\mathbb{W}_k)_R,\Delta x_L,\Delta x_R) = 2\pi_I^{\Delta}((\mathbb{W}_k)_L,(\mathbb{W}_k)_R)\frac{(\alpha_k)_R-(\alpha_k)_L}{\Delta x_L+\Delta x_R}. \tag{25}$$

By construction, the approximate Riemann solver defined by (21) and (25) verifies the three conditions 1), 2) and 3). We end up with the following update at the acoustic step:

$$\left\{\begin{array}{lcl}
(\alpha_k)_j^{\sharp} &=& (\alpha_1)_j^n,\\
(\tau_k)_j^{\sharp} &=& (\tau_k)_j^n + \frac{\Delta t}{\Delta x(\rho_k)_j^n}\left((u_k)_{j+1/2}^{\star}-(u_k)_{j-1/2}^{\star}\right),\\
(u_k)_j^{\sharp} &=& (u_k)_j^n - \frac{\Delta t}{\Delta x(\alpha_k\rho_k)_j^n}\left((\alpha_k\pi_k)_{j+1/2}^{\star}-(\alpha_k\pi_k)_{j-1/2}^{\star}\right) + \frac{\Delta t}{(\alpha_k\rho_k)_j^n}\left\{\pi_I\partial_x\alpha_k\right\}_j^n,\\
(\pi_k)_j^{\sharp} &=& (\pi_k)_j^n - \frac{\Delta t}{\Delta x(\rho_k)_j^n}a_k^2\left((u_k)_{j+1/2}^{\star}-(u_k)_{j-1/2}^{\star}\right),
\end{array}\right. \tag{26}$$

where $(\pi_k)_j^n = p_k^{EOS}((\tau_k)_j^n)$ and

- $\overline{\alpha_k}_{j+1/2}(u_k)_{j+1/2}^{\star} = \overline{\alpha_k u_k}_{j+1/2} - \frac{\Delta(\alpha_k\pi_k)}{2a_k} + \frac{1}{2a_k}\left\{S_k\right\}_{j+1/2}^n$,
- $\overline{\alpha_k}_{j+1/2}(\alpha_k\pi_k)_{j+1/2}^{\star} = (\alpha_k)_j(\alpha_k)_{j+1}\left(\overline{\pi_k}-\frac{a_k}{2}\Delta u_k\right) + \frac{\Delta\alpha_k}{4}\left\{S_k\right\}_{j+1/2}^n$,
- $\left\{S_k\right\}_j^n = \frac{1}{2}\left\{S_k\right\}_{j+1/2}^n + \frac{1}{2}\left\{S_k\right\}_{j-1/2}^n$, with: $\left\{S_k\right\}_{j+1/2}^n = \overline{\pi_I}_{j+1/2}\Delta(\alpha_k)_{j+1/2}$,

where: $\overline{b}_{j+1/2} = \frac{b_{j+1}+b_j}{2}$, $\quad \Delta b_{j+1/2} = b_{j+1}-b_j$.

4.2. **Treatment of the second step**

We now consider the numerical treatment of the time evolution corresponding to the second step. Starting from the output of the first step $\mathbb{U}_j^{\sharp}$, we want to compute the updated data at time t^{n+1}, $\mathbb{U}_j^{n+1}$. Denoting $\phi_k \in \{m_k, m_k u_k\}$, we use a standard time-explicit upwind discretization for the transport step by setting

$$\begin{array}{rcllll}
(\phi_k)_j^{n+1} &=& (\phi_k)_j^{\sharp} &-& \frac{\Delta t}{\Delta x}\left((u_k)_{j+1/2}^{\star}(\phi_k)_{j+1/2}^{\sharp}-(u_k)_{j-1/2}^{\star}(\phi_k)_{j-1/2}^{\sharp}\right)\\
& & &+& \frac{\Delta t}{\Delta x}(\phi_k)_j^{\sharp}\left((u_k)_{j+1/2}^{\star}-(u_k)_{j-1/2}^{\star}\right),\\
(\alpha_k)_j^{n+1} &=& (\alpha_k)_j^{\sharp} &-& \frac{\Delta t}{\Delta x}\left((u_I)_{j+1/2}^{\star}(\alpha_k)_{j+1/2}^{\sharp}-(u_I)_{j-1/2}^{\star}(\alpha_k)_{j-1/2}^{\sharp}\right)\\
& & &+& \frac{\Delta t}{\Delta x}(\alpha_k)_j^{\sharp}\left((u_I)_{j+1/2}^{\star}-(u_I)_{j-1/2}^{\star}\right),
\end{array} \tag{27}$$

where

$$(\phi_k)_{j+1/2}^{\sharp} = \left\{\begin{array}{ll}(\phi_k)_j^{\sharp}, & \text{if } (u_k)_{j+1/2}^{\star}\geq 0,\\ (\phi_k)_{j+1}^{\sharp}, & \text{if } (u_k)_{j+1/2}^{\star}<0\end{array}\right., \quad (\alpha_k)_{j+1/2}^{\sharp} = \left\{\begin{array}{ll}(\alpha_k)_j^{\sharp}, & \text{if } (u_I)_{j+1/2}^{\star}\geq 0,\\ (\alpha_k)_{j+1}^{\sharp}, & \text{if } (u_I)_{j+1/2}^{\star}<0\end{array}\right..$$

Let us note that the transport update (27) equivalently reads:

$$\begin{array}{rcl}(\phi_k)_j^{n+1} &=& (\phi_k)_j^\sharp L_j - \frac{\Delta t}{\Delta x}\left((u_k)^\star_{j+1/2}(\phi_k)^\sharp_{j+1/2} - (u_k)^\star_{j-1/2}(\phi_k)^\sharp_{j-1/2}\right),\\ (\alpha_k)_j^{n+1} &=& (\alpha_k)_j^\sharp L_j^I - \frac{\Delta t}{\Delta x}\left((u_I)^\star_{j+1/2}(\alpha_k)^\sharp_{j+1/2} - (u_I)^\star_{j-1/2}(\alpha_k)^\sharp_{j-1/2}\right),\\ L_j^I &=& 1 + \frac{\Delta t}{\Delta x}\left((u_I)^\star_{j+1/2} - (u_I)^\star_{j-1/2}\right).\end{array} \tag{28}$$

Let us note that the interface value of the velocity $(u_k)^\star_{j+1/2}$ coincides with the one proposed in the first step, which is actually crucial in order for the whole scheme to be conservative.

5. Two-step numerical method

In this section, we now give the details of the two-step process proposed in Section 3 for solving the barotropic Baer Nunziato model. Let us briefly recall that this two-step process is defined by

- Update $\mathbb{U}_j^n$ to $\mathbb{U}_j^\sharp$ by approximating the solution of (7).
- Update $\mathbb{U}_j^\sharp$ to $\mathbb{U}_j^{n+1}$ by approximating the solution of (13).

In the sequel, if we assume as given the approximate solution $\{\mathbb{U}_j^n\}_j$ at time t^n, we introduce the approximate solution $\{\mathbb{W}_j^n\}_j$ at equilibrium in the $\mathbb{W}$ variable. We begin with a fully explicit discretization of the Baer Nunziato model, which means that both steps of the process are solved with a time-explicit procedure, and we will go on with a mixed implicit-explicit strategy for which the solutions of (7) are solved implicitly in time and the solutions of (13) are solved explicitly. The latter strategy allows to get rid of the strong CFL restriction coming from the acoustic waves in the subsonic regime and corresponds to the motivation of the present study.

5.1. Time-explicit discretization

Let us begin with the time-explicit discretization of the acoustic system (7), or equivalently (9). The acoustic update is achieved thanks to the proposed relaxation approximation and the corresponding approximate Riemann solver detailed in Section 4.1. More precisely, we propose to simply use a Godunov-type method based on this approximate Riemann solver. If we focus on the conservative variable: $(\alpha_k, m_k, m_k u_k, \rho_k \pi_k)$, the discretization (26) yields the following formula for the acoustic update:

$$\left\{\begin{array}{rcl}(\alpha_k)_j^\sharp &=& (\alpha_1)_j^n,\\ L_j(m_k)_j^\sharp &=& (m_k)_j^n,\\ L_j(m_k u_k)_j^\sharp &=& (m_k u_k)_j^n - \frac{\Delta t}{\Delta x}\left((\alpha_k\pi_k)^\star_{j+1/2} - (\alpha_k\pi_k)^\star_{j-1/2}\right) + \Delta t\left\{\pi_I \partial_x \alpha_k\right\}_j^n,\\ L_j(\rho_k\pi_k)_j^\sharp &=& (\rho_k\pi_k)_j^n - \frac{\Delta t}{\Delta x} a_k^2\left((u_k)^\star_{j+1/2} - (u_k)^\star_{j-1/2}\right),\\ L_j &=& 1 + \frac{\Delta}{\Delta x}\left((u_k)^\star_{j+1/2} - (u_k)^\star_{j-1/2}\right).\end{array}\right. \tag{29}$$

Overall Discretization After injecting (29) in (28) one obtains the complete update procedure from t^n to t^{n+} for the conservative variables:

$$\left\{\begin{array}{rcl}(\alpha_k)_j^{n+1} &=& (\alpha_k)_j^\sharp L_j^I - \frac{\Delta t}{\Delta x}\left((u_I)^\star_{j+1/2}(\alpha_k)^\sharp_{j+1/2} - (u_I)^\star_{j-1/2}(\alpha_k)^\sharp_{j-1/2}\right),\\ (m_k)_j^{n+1} &=& (m_k)_j^n - \frac{\Delta t}{\Delta x}\left((u_k)^\star_{j+1/2}(m_k)^\sharp_{j+1/2} - (u_k)^\star_{j-1/2}(m_k)^\sharp_{j-1/2}\right),\\ (m_k u_k)_j^{n+1} &=& (m_k u_k)_j^n - \frac{\Delta t}{\Delta x}\left((u_k)^\star_{j+1/2}(m_k u_k)^\sharp_{j+1/2} + (\alpha_k\pi_k)^\star_{j+1/2}\right.\\ &-& \left.(u_k)^\star_{j-1/2}(m_k u_k)^\sharp_{j-1/2} - (\alpha_k\pi_k)^\star_{j-1/2}\right) + \Delta t\left\{\pi_I\partial_x\alpha_k\right\}_j^n,\\ L_j^I &=& 1 + \frac{\Delta}{\Delta x}\left((u_I)^\star_{j+1/2} - (u_I)^\star_{j-1/2}\right).\end{array}\right. \tag{30}$$

The next statement gather the main properties satisfied by our explicit in time and two-step algorithm.

Proposition 5.1. *The fully explicit scheme (26)-(27) satisfies the following:*

- *The discretization of the partial masses m_k is conservative*
- *The discretization of the total momentum $m_1u_1 + m_2u_2$ is conservative.*
- *The constant velocities/pressures profiles are preserved.*

Under the Whitham subcharacteristic condition and the CFL conditions,

$$\frac{\Delta t}{\Delta x}\max_{j\in\mathbb{Z}}\max_{k\in\{1,2\}}|\,(a_k\tau_k)_j^n\,|<\frac{1}{2},\quad \frac{\Delta t}{\Delta x}\max_{j\in\mathbb{Z}}\left(((u_k)^\star_{j-1/2})^+-((u_k)^\star_{j+1/2})^-\right)<1 \tag{31}$$

- *It preserves the maximum principle for the phase fractions: $0<\alpha_k<1$ and positive values of the densities $\rho_k>0$.*

Proof.

- This is a straightforward consequence of (30).
- Summing the momentum equations in system (30) over k yields:

$$\begin{aligned}(m_1u_1+m_2u_2)_j^{n+1} &= (m_1u_1+m_2u_2)_j^n-\tfrac{\Delta t}{\Delta x}\Big((\alpha_1\pi_1+\alpha_2\pi_2)^{\star L}_{j+1/2}-(\alpha_1\pi_1+\alpha_2\pi_2)^{\star R}_{j-1/2}\\ &+ (u_1)^\star_{j+1/2}(m_1u_1)^\sharp_{j+1/2}-(u_1)^\star_{j-1/2}(m_1u_1)^\sharp_{j-1/2}\\ &+ (u_2)^\star_{j+1/2}(m_2u_2)^\sharp_{j+1/2}-(u_2)^\star_{j-1/2}(m_2u_2)^\sharp_{j-1/2}\Big).\end{aligned}$$

  As $\alpha_1\pi_1+\alpha_2\pi_2$ is a Riemann invariant of the standing wave for the relaxation acoustic system (10), we have $(\alpha_1\pi_1+\alpha_2\pi_2)^{\star L}_{j+1/2}=(\alpha_1\pi_1+\alpha_2\pi_2)^{\star R}_{j+1/2}$, which preserves the conservative form.
- Let us consider the state:

$$\big((\alpha_1)_j^n,(\tau_1)_j^n,(u_1)_j^n,(p_1)_j^n,(\tau_2)_j^n,(u_2)_j^n,(p_2)_j^n\big)=\big((\alpha_1)_j^n,\overline{\tau},\overline{u},\overline{p},\overline{\tau},\overline{u},\overline{p}\big),\quad (\alpha_1)_j^n\in(0,1),$$

  with constant velocities $\overline{u}$ and pressures $\overline{p}$. Injecting this state in the two-step numerical method (30), we obtain:

$$\big((\alpha_1)_j^{n+1},(\tau_1)_j^{n+1},(u_1)_j^{n+1},(p_1)_j^{n+1},(\tau_2)_j^{n+1},(u_2)_j^{n+1},(p_2)_j^{n+1}\big)=\big((\alpha_1)_j^{n+1},\overline{\tau},\overline{u},\overline{p},\overline{\tau},\overline{u},\overline{p}\big),\quad (\alpha_1)_j^{n+1}\in(0,1).$$

- Thanks to (29), the CFL condition (31) ensures that $(\rho_k)_j^\sharp>0$ and $0<(\alpha_k)_j^\sharp<1$ for $j\in\mathbb{Z}$. The CFL condition (31) yields that $(\rho_k)_j^{n+1}$ and $(\alpha_k)_j^{n+1}$ are convex combinations of $(\rho_k)_l^\sharp$ and $(\alpha_k)_l^\sharp$ respectively for $l=j\pm1,j$ and therefore $(\rho_k)_j^{n+1}>0$ and $0<(\alpha_k)_j^{n+1}<1$.

□

5.2. **Semi-implicit discretization**

Let us now consider the last algorithm of this paper, which consists in considering a time-implicit scheme for the acoustic step and keeping unchanged the transport step. This strategy will allow us to obtain a stable algorithm under a CFL restriction based on the material velocity u_k and not on the sound velocity c_k. In order to derive a time-implicit scheme for the acoustic step, we follow the following standard approach where the numerical fluxes are now evaluated at time $t^\sharp$, which gives here the same update formulas as in the explicit case but where the numerical fluxes now involve quantities at time $t^\sharp$ apart from the term consistent with $\{\pi_I\partial_x\alpha_k\}$, which writes:

- $\overline{\alpha_k}_{j+1/2}((u_k)^\star_{j+1/2})^\sharp=\overline{\alpha_k u_k}^\sharp_{j+1/2}-\frac{\Delta(\alpha_k\pi_k)^\sharp}{2a_k}+\frac{1}{2a_k}\{S_k\}^n_{j+1/2}$,
- $\overline{\alpha_k}_{j+1/2}((\alpha_k\pi_k)^\star_{j+1/2})^\sharp=(\alpha_k)_j(\alpha_k)_{j+1}\left(\overline{\pi_k}^\sharp-\frac{a_k}{2}\Delta u_k^\sharp\right)+\frac{\Delta\alpha_k}{4}\{S_k\}^n_{j+1/2}$.

Let us observe that we suggest here to keep on evaluating the interfacial pressure source term at time t^n. It is interesting to see that it is equivalent to the following system written in characteristic variables:

$$\begin{aligned}
(\alpha_1)_j^\sharp &= (\alpha_1)_j^n, \\
(\tau_k)_j^\sharp &= (\tau_k)_j^n + \frac{\lambda}{(\rho_k)_j^n}\left((u_k^\star)_{j+1/2}^\sharp - (u_k^\star)_{j-1/2}^\sharp\right), \\
(\overrightarrow{W}_k)_j^\sharp &= (\overrightarrow{W}_k)_j^n - \frac{\lambda a_k}{(\rho_k)_j^n}(\overrightarrow{W}_k)_j^\sharp + \frac{\lambda a_k(\alpha_k)_{j-1}^n}{(\rho_k)_j^n(\overline{\alpha_k})_{j-1/2}}(\overrightarrow{W}_k)_{j-1}^\sharp - \frac{\lambda a_k(\Delta\alpha_k)_{j-1/2}}{2(\rho_k)_j^n(\overline{\alpha_k})_{j-1/2}}(\overleftarrow{W}_k)_j^\sharp \\
&+ \frac{\lambda a_k}{(\overline{\alpha_k})_{j-1/2}(\rho_k)_j^n}\{S\}_{j-1/2}^n, \\
(\overleftarrow{W}_k)_j^\sharp &= (\overleftarrow{W}_k)_j^n - \frac{\lambda a_k}{(\rho_k)_j^n}(\overleftarrow{W}_k)_j^\sharp + \frac{\lambda a_k(\alpha_k)_{j+1}^n}{(\rho_k)_j^n(\overline{\alpha_k})_{j+1/2}}(\overleftarrow{W}_k)_{j+1}^\sharp + \frac{\lambda a_k(\Delta\alpha_k)_{j+1/2}}{2(\rho_k)_j^n(\overline{\alpha_k})_{j+1/2}}(\overrightarrow{W}_k)_j^\sharp \\
&- \frac{\lambda a_k}{(\overline{\alpha_k})_{j+1/2}(\rho_k)_j^n}\{S\}_{j+1/2}^n,
\end{aligned} \tag{32}$$

where the new variables $\overleftarrow{W}_k$ and $\overrightarrow{W}_k$ are defined by $\overrightarrow{W}_k = \pi_k + a_k u_k$, $\overleftarrow{W}_k = \pi_k - a_k u_k$. These quantities are the Riemann invariants associated with the characteristic speeds $\pm a_k\tau_k$ of the relaxation system (12). We firstly compute $\overleftarrow{W}_k$ and $\overrightarrow{W}_k$. Once this is done, τ_k variables can be updated explicitly since $((u_k)_{j\pm1/2}^\star)^\sharp$ is explicitly known from the knowledge of $\overleftarrow{W}_k^{\ \sharp}$ and $\overrightarrow{W}_k^{\ \sharp}$ by the formulas

$$(u_k)_j^\sharp = \frac{1}{2a_k}\left((\overrightarrow{W}_k)_j^\sharp - (\overleftarrow{W}_k)_j^\sharp\right), \qquad (\pi_k)_j^\sharp = \frac{1}{2}\left((\overrightarrow{W}_k)_j^\sharp + (\overleftarrow{W}_k)_j^\sharp\right).$$

Remark 5.2. In the semi-implicit Lagrange projection, we need to solve a linear system to update the solution at time $t^\sharp$.

$$\begin{pmatrix} A_{\overrightarrow{W}_k,\overrightarrow{W}_k} & A_{\overrightarrow{W}_k,\overleftarrow{W}_k} \\ A_{\overleftarrow{W}_k,\overrightarrow{W}_k} & A_{\overleftarrow{W}_k,\overleftarrow{W}_k} \end{pmatrix} \begin{pmatrix} \overrightarrow{W}_k \\ \overleftarrow{W}_k \end{pmatrix} = \begin{pmatrix} B_{\overrightarrow{W}_k} \\ B_{\overleftarrow{W}_k} \end{pmatrix}, \tag{33}$$

where the block matrices $A_{\overrightarrow{W}_k,\overrightarrow{W}_k}$ and $A_{\overleftarrow{W}_k,\overleftarrow{W}_k}$ are bidiagonal and the block matrices $A_{\overrightarrow{W}_k,\overleftarrow{W}_k}$ and $A_{\overleftarrow{W}_k,\overrightarrow{W}_k}$ are diagonal. The implementation of this sparse matrix is made by the use of the Python library "*scipy.sparse*" and we solve the linear system (33) with a direct method from "*scipy.sparse.spsolve*".

Proposition 5.3. *The implicit-explicit scheme (32)-(27) satisfies the following:*

- *The discretization of the partial masses m_k is conservative*
- *The discretization of the total momentum $m_1u_1 + m_2u_2$ is conservative.*
- *The constant velocities/pressures profiles are preserved.*

Under the Whitham subcharacteristic condition and the CFL conditions,

$$\frac{\Delta t}{\Delta x}\max_{j\in\mathbb{Z}}\left(((u_k)_{j-1/2}^\star)^+ - ((u_k)_{j+1/2}^\star)^-\right) < 1 \tag{34}$$

- *It preserves the maximum principle for the phase fractions: $0 < \alpha_k < 1$ and positive values of the densities $\rho_k > 0$.*

Proof. The properties are obtained in the same way as in the explicit case. □

6. Numerical results

In this section, we present three test cases that are representative of the numerical challenges of the BN model: the vanishing phase and the capture of a pure contact discontinuity. Here, we compare the approximate solution, computed with our two-step numerical scheme, with a reference solution.

In these cases, the phasic equations of state are given by the following ideal gas pressure laws:

$$\begin{array}{c} p_1(\rho_1) = \kappa_1 \rho_1^{\gamma_1}, \text{ with } \kappa_1 = 1 \text{ and } \gamma_1 = 3, \\ p_2(\rho_2) = \kappa_2 \rho_2^{\gamma_2}, \text{ with } \kappa_2 = 1 \text{ and } \gamma_1 = 1.5. \end{array} \tag{35}$$

The solutions are computed on the domain $[0, 1]$ of the x-space.

6.1. **Test case 1: a complete Riemann problem**

We consider a first test that displays all the waves: acoustic waves and contact discontinuity, with the following initial data [11],

$$\begin{array}{rcl} U_L & = & (0.1, 0.85, 0.4609513139, 0.96, 0.0839315299) \text{ if } x < 0, \\ U_R & = & (0.6, 1.2520240113, 0.7170741165, 0.2505659851, -0.3764790609) \text{ if } x > 0. \end{array}$$

The exact solution is composed of a $(u_1 - c_1)$-shock wave, followed by a $(u_2 - c_2)$-rarefaction wave, followed by a u_2-contact discontinuity, followed by a $(u_2 + c_2)$-shock and finally followed by a $(u_1 + c_1)$-rarefaction wave.

In Figures 1, 2, the approximate solution computed with the explicit and implicit-explicit Lagrange projection schemes are compared with both a reference solution computed over a 10^5 cells mesh with the Rusanov scheme and the approximate solution obtained with Rusanov scheme. We first observe that the implicit scheme is the most diffusive, which was clearly expected from the implicit treatment of the acoustic step. Note also that our Lagrange-Projection schemes correctly capture the intermediate states even for this rather coarse mesh of 1000 cells. It appears that the contact discontinuity is captured more sharply by the explicit Lagrange projection method than by Rusanov scheme for which the numerical diffusion is larger. The two Lagrange projection schemes are comparable to the results given by the relaxation scheme introduced in [12] (see page 34). Nevertheless, we observe that the ImEx method generates an overshoot at the contact discontinuity where the phase fraction α_k jumps. This oscillation is reduced on a finer mesh of 10000 cells in Figure 2 and does not generate an instability. To have a better understanding of this behavior at the contact discontinuity, we study a Riemann problem with a stationnary contact discontinuity in the last test case. The appearance of all the waves in this first test case and of their numerical diffusion can make the interpretation of the results difficult. Table 1 gives for each test case the number of iterations needed to perform the computations. As expected, the gain is important when using the proposed implicit-explicit algorithm and the corresponding CFL restriction based on the material waves (instead of the acoustic waves as for the explicit scheme).

	Test 1	Test 2	Test 3
Rusanov	808	780	688
LP explicit	616	729	672
LP implicit	203	214	398

Table 1. Number of time-iterations for each test case with 1000 cells

6.2. **Test case 2: vanishing phase**

We now consider a Riemann problem in which one of the two phases vanishes in one of the initial states, which means that the corresponding phase fraction α_1 or α_2 is equal to zero. This configuration poses a difficulty in the two-fluid model owing to its independent velocities. The singularity arises when one computes the absent

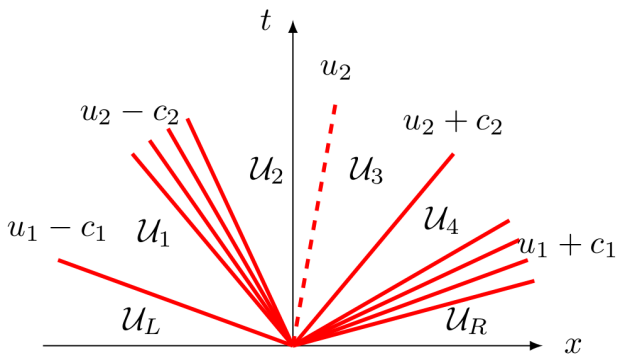

(A) Wave structure of the exact Riemann solution

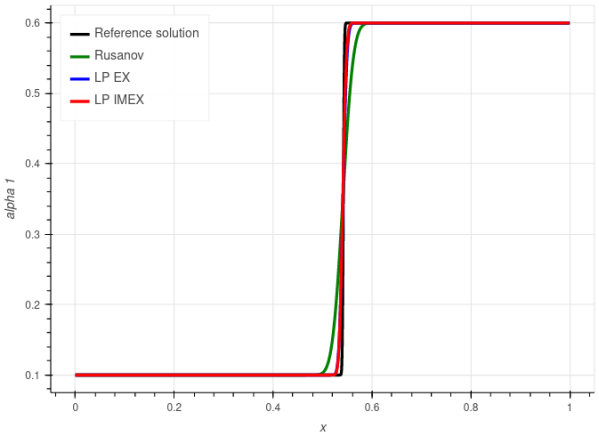

(B) Phase 1 fraction α_1

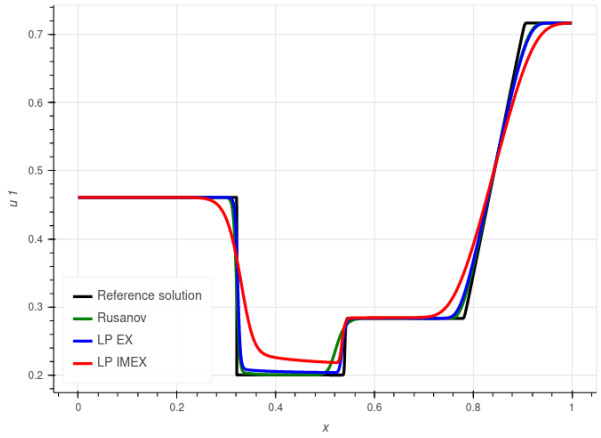

(C) Phase 1 velocity u_1

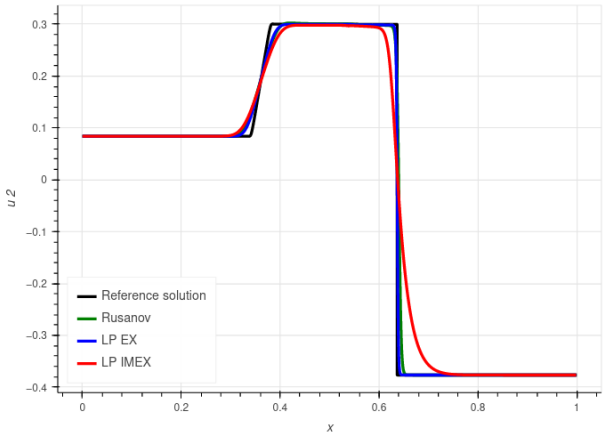

(D) Phase 2 velocity u_2

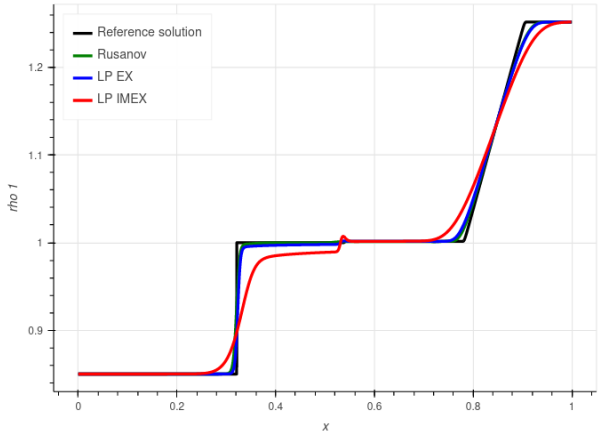

(E) Phase 1 density ρ_1

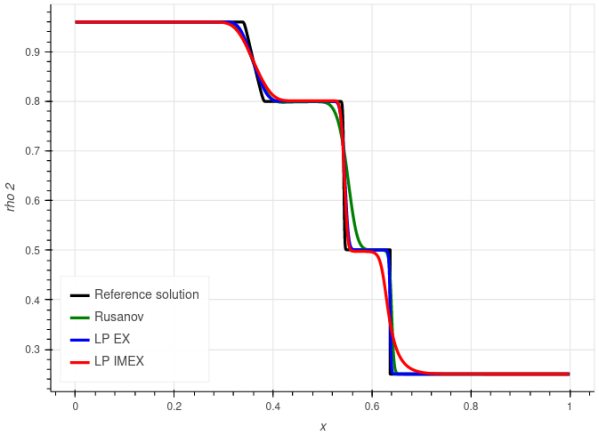

(F) Phase 2 density ρ_2

FIGURE 1. Test case 1: Structure of the solution and space variations of the physical variables at the final time $T = 0.14$. Mesh size: 1000 cells.

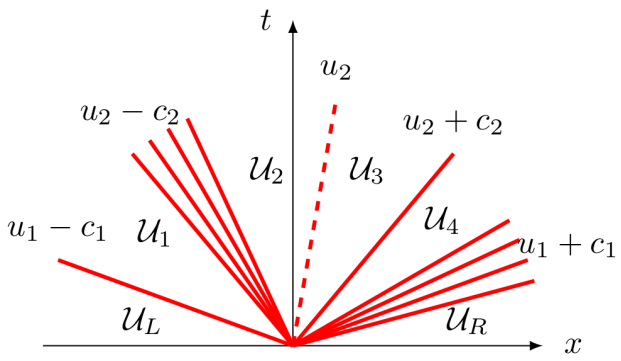

(A) Wave structure of the exact Riemann solution

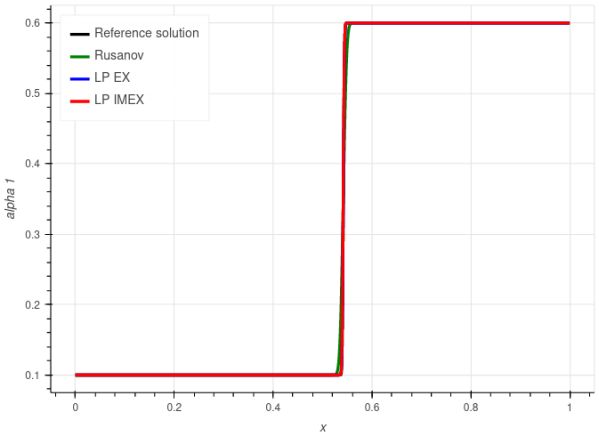

(B) Phase 1 fraction α_1

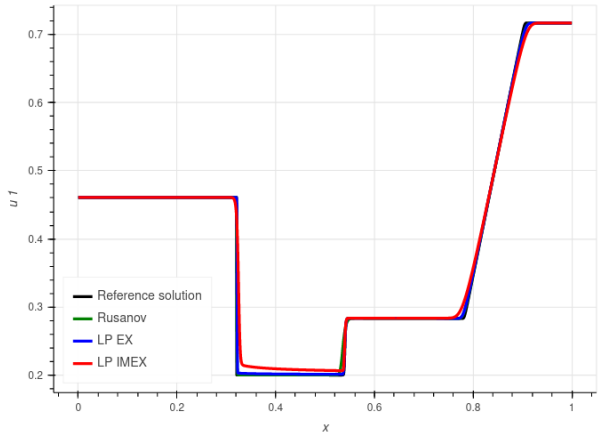

(C) Phase 1 velocity u_1

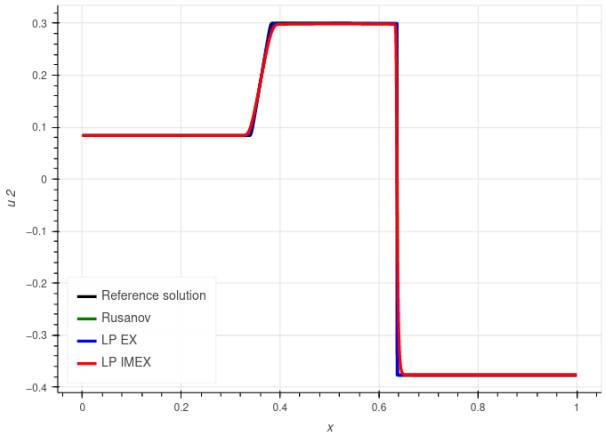

(D) Phase 2 velocity u_2

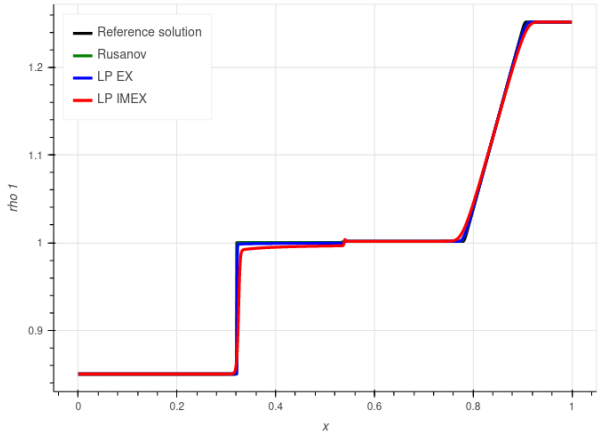

(E) Phase 1 density ρ_1

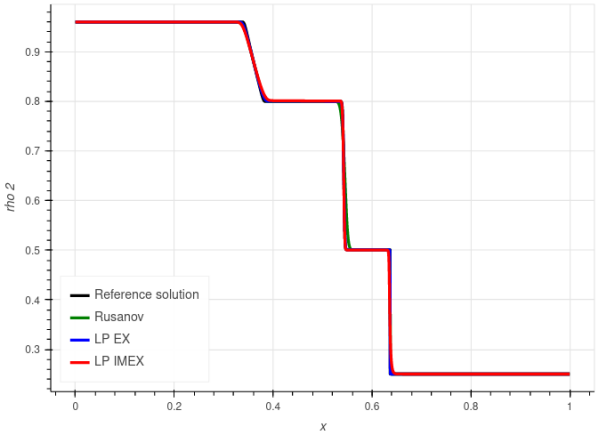

(F) Phase 2 density ρ_2

FIGURE 2. Test case 1: Structure of the solution and space variations of the physical variables at the final time $T = 0.14$. Mesh size: 10000 cells.

phase velocity using the conservative variables $u_k = \frac{\alpha_k \rho_k u_k}{\alpha_k \rho_k}$.
For this kind of Riemann problem, the u_I-contact separates a mixture region where the two phases coexist from a single phase region with the remaining phase. Assuming for instance that $\alpha_1^L = 1$ and $0 < \alpha_1^R < 1$, the right state is a mixture of both phases while the left initial state is composed solely of phase 1. We consider the following initial data [11],

$$\begin{aligned} U_L &= (1, 1.8, 0.747051068928543, 3.979765198025580, 0.6) \text{ if } x < 0, \\ U_R &= (0.4, 2.081142099494683, 0.267119045902047, 5.173694757433254, 1.069067604724276) \text{ if } x > 0. \end{aligned}$$

The exact solution is composed of a $(u_1 - c_1)$-shock wave in the left-hand side region where only phase 1 is present. This region is separated by a u_I-contact discontinuity from the right-hand side region where the two phases are mixed. In this RHS region, the solution is composed of a $(u_2 + c_2)$-rarefaction wave followed by a $(u_1 + c_1)$-rarefaction wave. In practice, the numerical method requires values of α_1^L and α_1^R that lie strictly in the interval $(0, 1)$. Therefore, in the numerical implementation, we take $\alpha_1^L = 1 - 10^{-9}$. The aim here is to give a qualitative comparison between the numerical approximation and the reference solution. Moreover, there is theoretically no need to specify left initial values for the phase 2 quantities since this phase is not present in the LHS region. For the sake of the numerical simulations however, one must provide such values. We choose to set ρ_2^L and u_2^L to the values on the right of the u_I-contact discontinuity. As for the first test case, we can see in Figures 3,4 that for the same level of refinement, the explicit Lagrange projection scheme is more accurate than Rusanov scheme, which can be seen especially for phase 1. As regards the region where phase 2 does not exist, we can see that the three numerical schemes develop some oscillations when it comes to divisions by small values of α_2. This behavior is also observed with the relaxation scheme in [12] (see page 37). The ImEx method also generates an oscillation at the location where the phase fraction α_2 jumps and is more diffusive for the capture of the $(u_1 + c_1)$-rarefaction wave (see Phase 1 density in Figure 3). The oscillation and numerical diffusion are lower on a finer mesh of 10000 cells in Figure 2 and ImEx method converges towards the reference solution.

6.3. **Test case 3: a pure contact discontinuity**

In the last test case, we seek to analyze the behavior of the explicit and ImEx Lagrange Projection (LP) schemes and the Rusanov scheme for the capture of a pure stationnary contact discontinuity. This Riemann problem is built following the procedure explained in Appendix A. Here, in the exact solution, all the physical quantities are transported with the constant velocity $u_I = 0$. The initial data is defined as

$$\begin{aligned} U_L &= (0.8, 7.0710678118654755, 0.4448746176198241, 3.7907146169832258, 0) \text{ if } x < 0, \\ U_R &= (0.2, 3.1622776601683795, 3.979079545848609, 3.6840314986403864, 0) \text{ if } x > 0. \end{aligned}$$

Figures 5 and 6 show that the stationnary contact is not correctly captured by all the schemes: Rusanov, explicit and ImEx LP schemes. The explicit Lagrange Projection scheme is much more accurate than the Rusanov scheme especially for the approximation of the interfacial velocity $u_I = 0$. The ImEx scheme generates an additional error compared to the explicit: this can be explained by the truncation error made by the ImEx scheme that is greater than the one made by the explicit scheme. Note that, to our knowledge, there exists no solver that is able to capture exactly a moving contact discontinuity (see [15] for a finite volume scheme on a staggered grid that preserves some Riemann invariants and [20] for the capture of stationary contacts), and our scheme compares rather well with other schemes. In this test case, we have isolated the error made by the splitting method at the contact discontinuity. This error is present in the explicit LP scheme and is amplified with ImEx schemes due to its greater truncation error. Hence, the oscillations we observe in the two previous test cases with the ImEx scheme might be present even for the explicit scheme but are damped by the numerical diffusion of the other waves, in the explicit case. In future works, we would like to propose another splitting strategy that allows to reduce the error made by the ImEx scheme at the contact discontinuity.

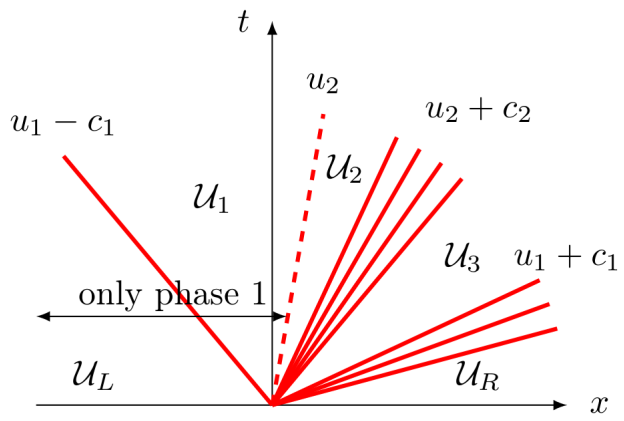

(A) Wave structure of the exact Riemann solution

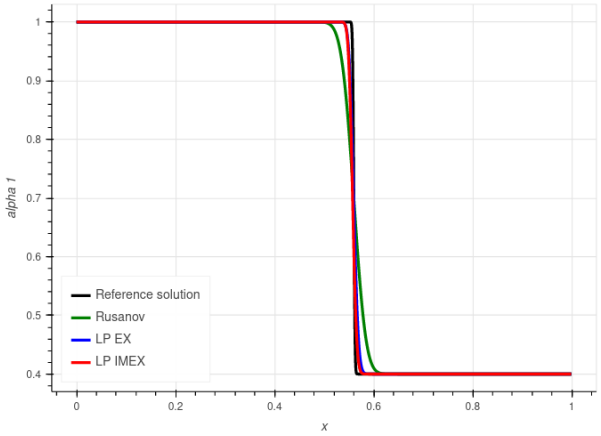

(B) Phase 1 fraction α_1

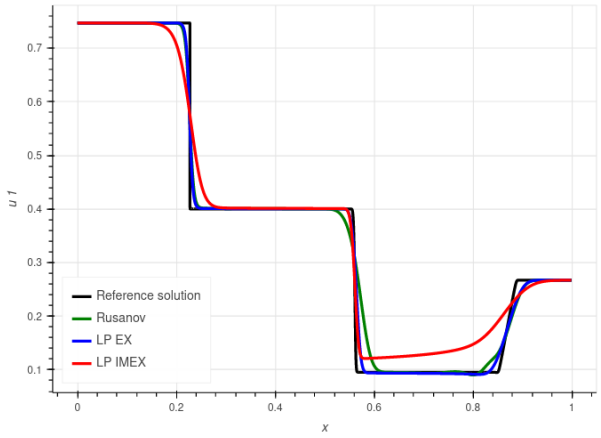

(C) Phase 1 velocity u_1

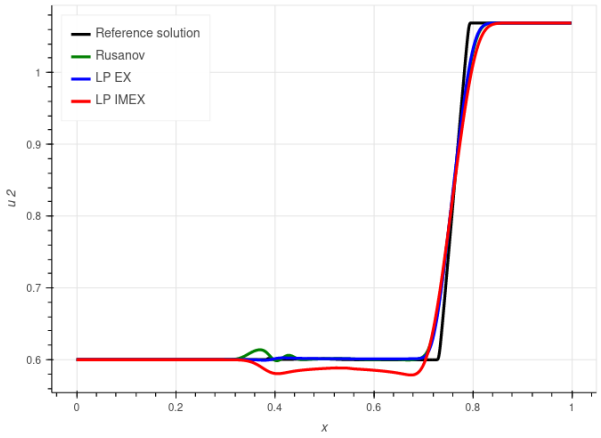

(D) Phase 2 velocity u_2

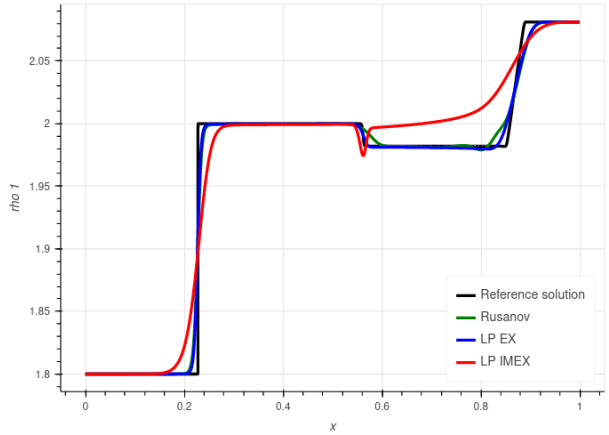

(E) Phase 1 density ρ_1

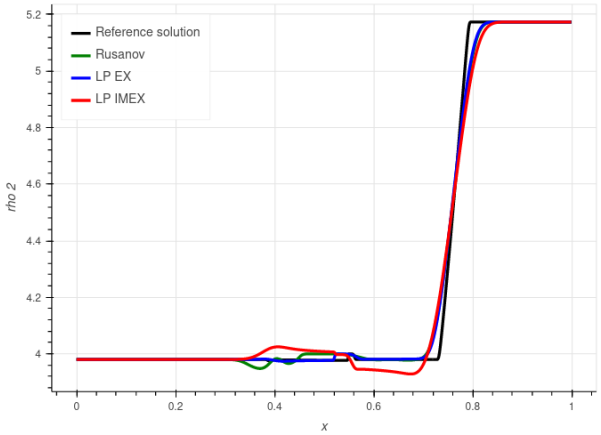

(F) Phase 2 density ρ_2

FIGURE 3. Test case 2: Structure of the solution and space variations of the physical variables at the final time $T = 0.1$. Mesh size: 1000 cells.

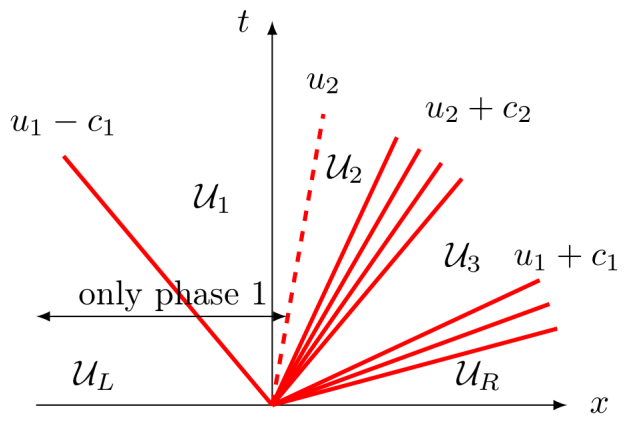

(A) Wave structure of the exact Riemann solution

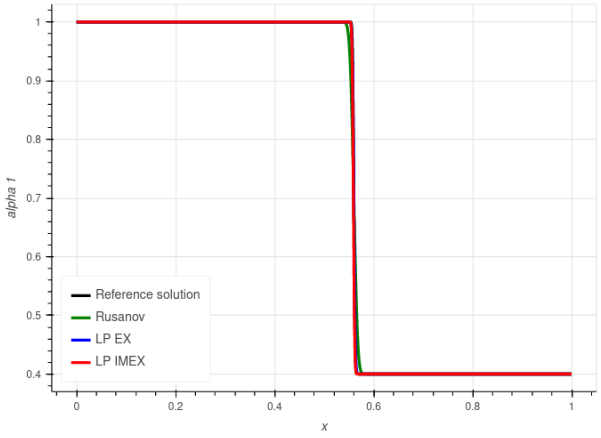

(B) Phase 1 fraction α_1

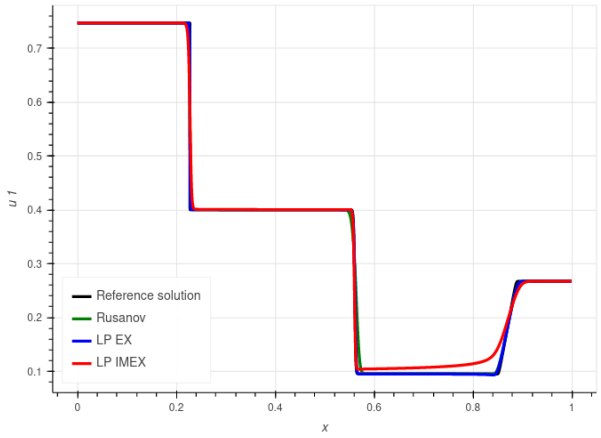

(C) Phase 1 velocity u_1

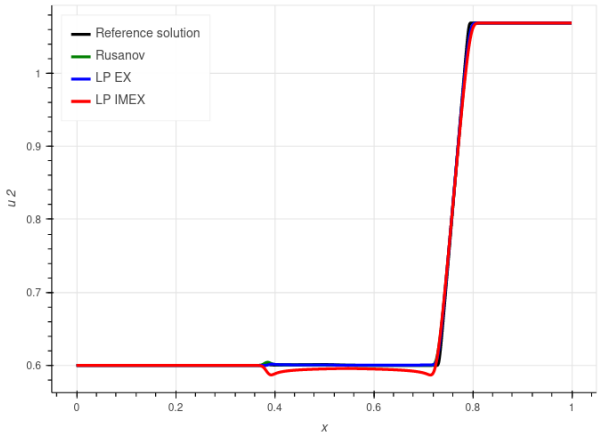

(D) Phase 2 velocity u_2

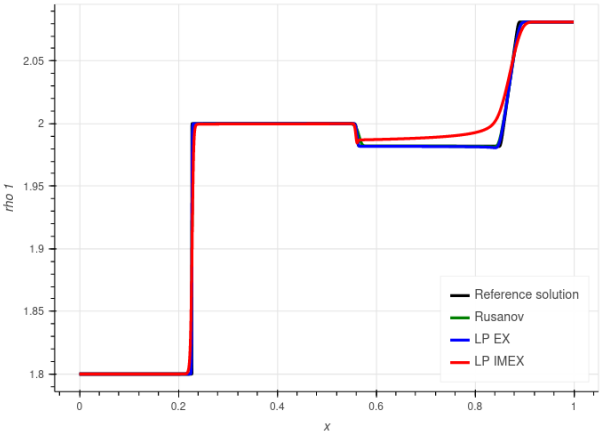

(E) Phase 1 density ρ_1

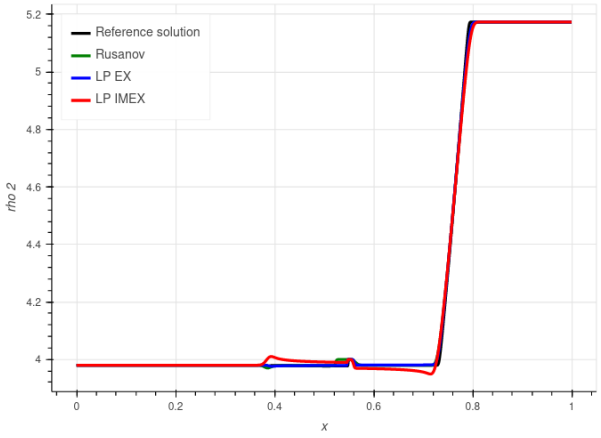

(F) Phase 2 density ρ_2

FIGURE 4. Test case 2: Structure of the solution and space variations of the physical variables at the final time $T = 0.1$. Mesh size: 10000 cells.

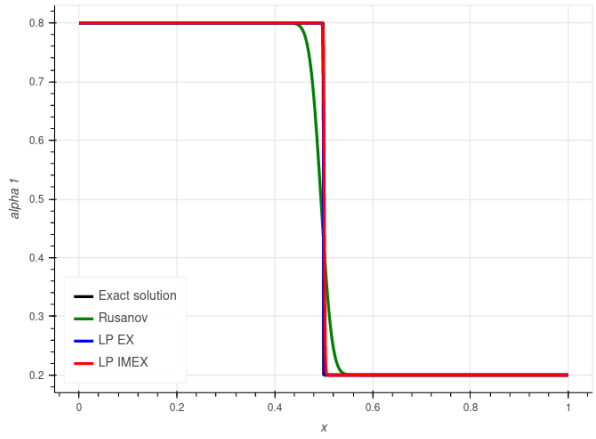

(A) Phase 1 fraction α_1

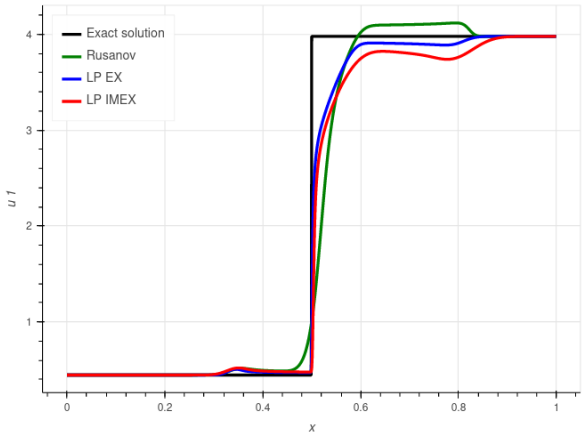

(B) Phase 1 velocity u_1

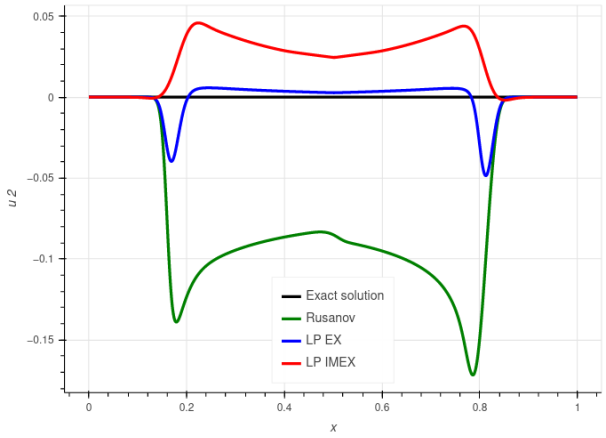

(C) Phase 2 velocity u_2

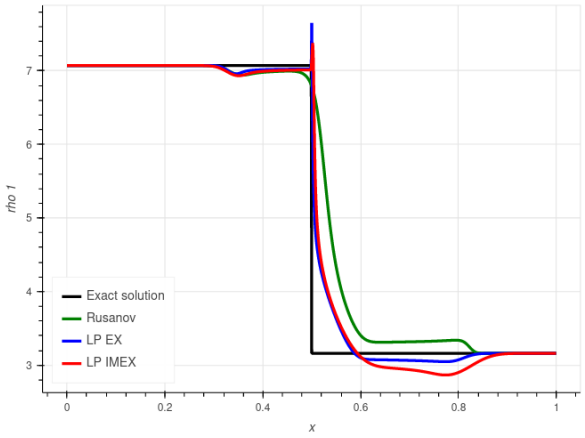

(D) Phase 1 density ρ_1

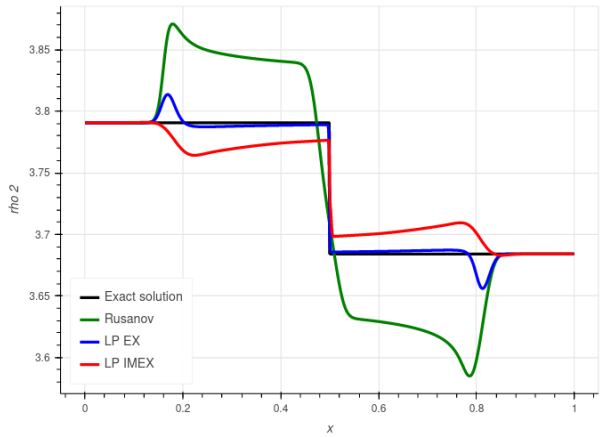

(E) Phase 2 density ρ_2

FIGURE 5. Test case 3: Structure of the solution and space variations of the physical variables at the final time $T = 0.05$. Mesh size: 1000 cells.

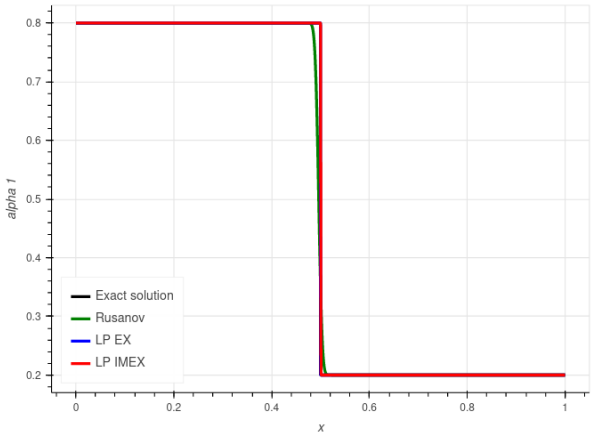

(A) Phase 1 fraction α_1

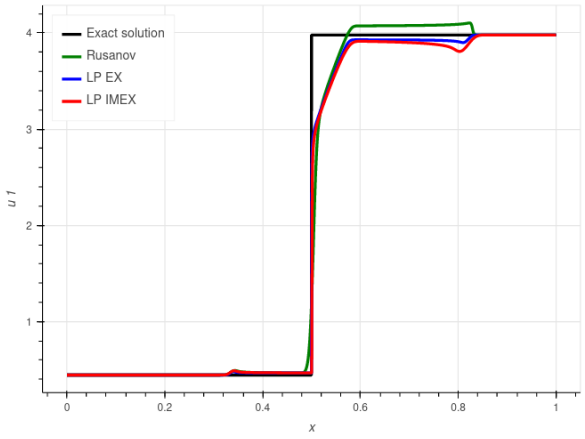

(B) Phase 1 velocity u_1

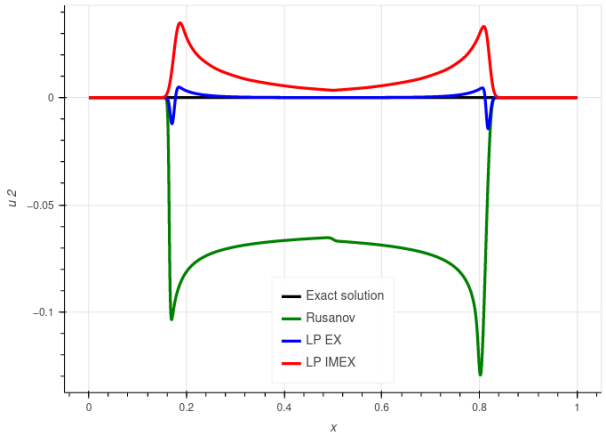

(C) Phase 2 velocity u_2

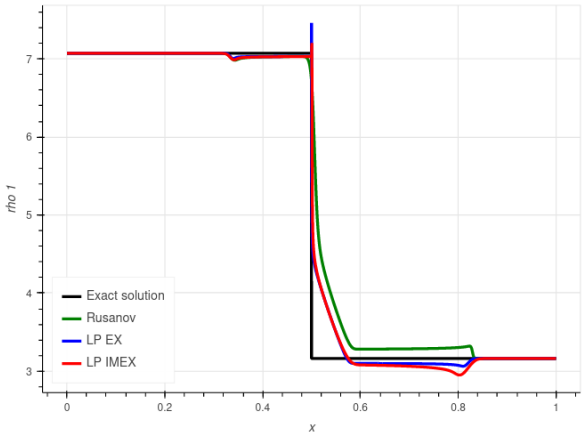

(D) Phase 1 density ρ_1

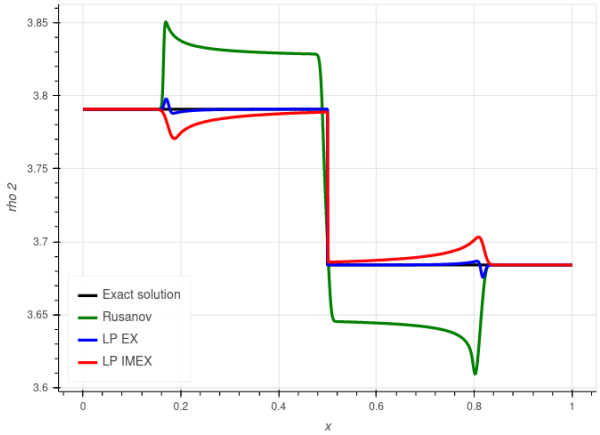

(E) Phase 2 density ρ_2

FIGURE 6. Test case 3: Structure of the solution and space variations of the physical variables at the final time $T = 0.05$. Mesh size: 10000 cells.

7. Conclusions

The explicit and implicit-explicit schemes presented here provide convergent aproximations of discontinuous solutions of the barotropic Baer-Nunziato model, while preserving the maximum principle on the values of the volume fractions α_k and positive values of the densities ρ_k . We have proposed a large time step scheme and proved stability properties under a time step CFL restriction based on the material velocities u_k and not on the sound velocities c_k as it is customary. The Lagrange-Projection decomposition proved to be efficient on a variety of test cases, but may be more diffusive than a direct Eulerian approach. We believe that the proposed implicit-explicit strategy is especially well adapted for subsonic flows but even more for low Mach numbers, which is our very motivation and the purpose of an ongoing work in several space dimensions. A sequel of this work consists in using the same fractional step strategy in order to derive an implicit-explicit numerical method for the Baer Nunziato model with energy equations, and thus to get rid of a rather constraining CFL condition due to the propagation of fast acoustic waves.

Acknowledgements

This work was supported by a grant from Région Ile-de-France DIM MATHINNOV and the project AID Écoles (École polytechnique, ENSTA, ONERA, CentraleSupélec) MMEED (Reduced-order multi-scale modeling of two-phase flows with strong couplings between phases: from primary atomization to turbulent dispersed-phase flows - PI. M. Massot and T. Pichard at École polytechnique and R. Monchaux at ENSTA) 2020-2024.

A. Riemann problem for the stationary contact discontinuity

In this section, we give a procedure to initialize a test case with a stationary contact discontinuity. We recall the Riemann invariants associated to the u_I contact discontinuity of the barotropic Baer Nunziato model:

$$u_I = u_2, \quad m_1(u_2-u_1), \quad m_1(u_2-u_1)^2 + \alpha_1 p_1 + \alpha_2 p_2, \quad \frac{(u_2-u_1)^2}{2} + e_1 + \frac{p_1}{\rho_1}. \tag{36}$$

We denote $[\![X]\!] = X_R - X_L$, the jump accross an interface where X_R and X_L are the right and left states. Hence we have the following set of jump relations:

$$[\![m_1 u_1]\!] = 0, \tag{37}$$

$$[\![m_1 u_1^2 + \sum_k \alpha_k p_k]\!] = 0, \tag{38}$$

$$[\![\frac{u_1^2}{2} + e_1 + \frac{p_1}{\rho_1}]\!] = 0. \tag{39}$$

From (37), we denote $\overline{m_1 u_1}$ such that: $\overline{m_1 u_1} = (m_1 u_1)_L = (m_1 u_1)_R$. From (39), we obtain:

$$\overline{m_1 u_1}^2 [\![\frac{1}{2\rho_1^2 \alpha_1^2}]\!] + [\![e_1 + \frac{p_1}{\rho_1}]\!] = 0. \tag{40}$$

We seek to define a test case where the initial condition is a stationary contact discontinuity. From given jumps $[\![\alpha_1]\!]$ and $[\![\rho_1]\!]$, we deduce the jumps $[\![\frac{1}{2\rho_1^2\alpha_1^2}]\!]$ and $[\![e_1 + \frac{p_1}{\rho_1}]\!]$. Assuming $\overline{m_1 u_1}$ is positive, we can compute its expression from (40). Starting from (38) and a given state $(p_2)_R$, we can deduce the left state $(p_2)_L$ with the following equation:

$$[\![m_1 u_1^2]\!] + [\![\alpha_1 p_1]\!] + (\alpha_2)_R (p_2)_R = (\alpha_2)_L (p_2)_L.$$

References

[1] A. Ambroso, C. Chalons, F. Coquel, and T. Galié. Relaxation and numerical approximation of a two-fluid two-pressure diphasic model. *ESAIM: Mathematical Modelling and Numerical Analysis - Modélisation Mathématique et Analyse Numérique*, 43(6):1063–1097, 2009.

[2] A. Ambroso, C. Chalons, and P.-A. Raviart. A Godunov-type method for the seven-equation model of compressible two-phase flow. *Computers & Fluids*, 54:67–91, 2012.

[3] N. Andrianov and G. Warnecke. The Riemann problem for the Baer-Nunziato two-phase flow model. *Journal of Computational Physics*, 195(2):434–464, 2004.

[4] M.R. Baer and J.W. Nunziato. A two-phase mixture theory for the deflagration-to-detonation transition DDT in reactive granular materials. *International Journal of Multiphase Flow*, 12(6):861–889, 1986.

[5] C. Chalons, F. Coquel, S. Kokh, and N. Spillane. Large Time-Step Numerical Scheme for the Seven-Equation Model of Compressible Two-Phase Flows. In *Finite Volumes for Complex Applications VI*, pages 225–233, 2011.

[6] C. Chalons and J.-F. Coulombel. Relaxation approximation of the Euler equations. *Journal of Mathematical Analysis and Applications*, 348(2):872–893, 2008.

[7] C. Chalons, M. Girardin, and S. Kokh. Large time step and asymptotic preserving numerical schemes for the gas dynamics equations with source terms. 35(6):A2874–A2902, 2013.

[8] C. Chalons, M. Girardin, and S. Kokh. An all-regime Lagrange-Projection like scheme for 2d homogeneous models for two-phase flows on unstructured meshes. *Journal of Computational Physics*, 335:885–904, 2017.

[9] C. Chalons, P. Kestener, S. Kokh, and M. Stauffert. A large time-step and well-balanced Lagrange-Projection type scheme for the shallow-water equations. *Communications in Mathematical Sciences*, 15(3):765–788, 2017.

[10] F. Coquel, E. Godlewski, and N. Seguin. Relaxation of fluid systems. *Mathematical Models and Methods in Applied Sciences*, 22(8):1250014, 2012.

[11] F. Coquel, J.-M. Hérard, and K. Saleh. A splitting method for the isentropic Baer Nunziato two-phase flow model. *ESAIM: Proceedings*, 38:241–256, 2012.

[12] F. Coquel, J.-M. Hérard, K. Saleh, and N. Seguin. A robust entropy-satisfying finite volume scheme for the isentropic Baer-Nunziato model. *ESAIM: Mathematical Modelling and Numerical Analysis - Modélisation Mathématique et Analyse Numérique*, 48(1):165–206, 2014.

[13] F. Coquel, Q. Nguyen, M. Postel, and Q.-H. Tran. Entropy-satisfying relaxation method with large time-steps for Euler IBVPs. *Mathematics of Computation*, 79:1493–1533, 2010.

[14] T. Gallouët, J.-M. Herard, and N. Seguin. Numerical modeling of two-phase flows using the two-fluid two-pressure approach. *Mathematical Models and Methods in Applied Sciences*, 14:663–700, 2004.

[15] X. Lei and J. Li. A staggered-projection Godunov-type method for the Baer-Nunziato two-phase model. *Journal of Computational Physics*, 437:110312, 2021.

[16] S. Peluchon, G. Gallice, and L. Mieussens. A robust implicit–explicit acoustic-transport splitting scheme for two-phase flows. *Journal of Computational Physics*, 339:328–355, 2017.

[17] D. W. Schwendeman, C. W. Wahle, and A. K. Kapila. The Riemann problem and a high-resolution Godunov method for a model of compressible two-phase flow. *Journal of Computational Physics*, 212(2):490–526, 2006.

[18] I. Suliciu. On the thermodynamics of rate-type fluids and phase transitions. I. rate-type fluids. *International Journal of Engineering Science*, 36:921–947, 1998.

[19] L. Tallois, S. Peluchon, and P. Villedieu. A second-order extension of a robust implicit–explicit acoustic-transport splitting scheme for two-phase flows. *Computers & Fluids*, 244:105531, 2022.

[20] M. Thanh, D. Kröner, and N. Nam. Numerical approximation for a Baer-Nunziato model of two-phase flows. *Applied Numerical Mathematics*, 61:702–721, 2011.

[21] S. A. Tokareva and E. F. Toro. HLLC-type Riemann solver for the Baer-Nunziato equations of compressible two-phase flow. *Journal of Computational Physics*, 229(10):3573–3604, 2010.

[22] Z. Zou, N. Grenier, S. Kokh, C. Tenaud, and E. Audit. Compressible solver for two-phase flows with sharp interface and capillary effects preserving accuracy in the low Mach regime. *Journal of Computational Physics*, 448:110735, 2022.